ENCOUNTER GEOMETRY AND SCIENCE DATA GATHERING SIMULATION

Meemong Lee
Raymond L. Swartz
Ansel Teng
Richard J. Weidner

Jet Propulsion Laboratory
California Institute of Technology
4800 Oak Grove Dr., Pasadena Ca. 91109

Abstract

Each space mission follows the process cycle of design, development, integration and test, launch and operation, science analysis and archive. The desire for more frequent and cost effective missions has motivated various new research and development efforts to reduce the design to launch period and the operation/analysis costs. With the revolutionary advances in information technology, the role of software simulation is becoming a very significant part of that pursuit. This paper presents a mission simulation software applied for design and validation of the MICAS observation sequence during the Deep Space 1 mission(DS1) of the New Millennium project . The mission simulation software integrates three systems, world, spacecraft, and observation system, in a distributed computing environment. The three systems are coordinated with a set of mission visualization tools for interactive control and comprehensive monitoring of the simulated mission. Major advantages of the integrated simulation system include inter-subsystem dependency and integrated impact simulation, subsystem-level performance requirement analysis, controlled propagation of subsystem-level uncertainties/errors, and high-fidelity mission data product generation.

1 Introduction

Modeling and Simulation is a fundamental part of scientific methods, which has guided the evolution of the science discipline. Modeling provides the continuity in science endeavor as a mechanism to express beliefs, hypotheses, or imaginations, to organize the current understandings, to analyze the observed phenomena, to predict future outcomes, and to update new discoveries.

Though the importance of modeling and simulation in mission design has been well acknowledged, a comprehensive system-level modeling and simulation was not feasible until recently. With the recent revolutionary advances in information technology in terms of computational power, computer graphics, and networking, modeling and simulation are becoming cost-effective tools for larger and more complex system design.

Mission Simulation and Instrument Modeling group at JPL, has been developing a comprehensive mission simulation software system [1] for generic science observation sequence design and validation. The mission simulation has been applied to several missions including Stardust/Discovery, Second Generation Micro-Spacecraft, and DSl/NewMillennium.

This paper discusses the mission simulation applied for DS1 /MICAS observation sequence design and validation. The DS 1 mision is planned to encounter an asteroid (McAulliffe), Mars, and a comet (West-Kohoutek-Ikcmura) during the two year mission period. The MICAS (Miniature Imaging Camera and Spectrometer) [1] is a primary payload system of the DS1 mission. MICAS has four detectors sharing the same optics: CCD (Charge-Coupled

Device), APS (Active Pixel Sensor), UV (Ultraviolet Spectrometer), and IR (Infrared Spectrometer). The effective field of views of the four detectors and their geometric relationship can be seen in the virtual camera view displayed in section 5.

Figure 1 depicts the relationship between the mission simulation and visualization. The mission simulation system is composed of three components: *World,* Spacecraft, and *Payload (Camera).* The three components contribute toward achieving the mission objective: *World,* the phenomena of the physical world the payload system will observe; *Spacecraft,* the geometric state control and estimation; and *Payload* (Camera), the observing system's performance and data product synthesis. Mission visualization monitors the inter-component relationship during the simulation employing three interactively controlled visualizers: trajectory, spacecraft, and virtual camera. The Sections 2, 3,and 4 discusses the three components of the mission simulation system in relation to encounter geometry and science data gathering simulation and the section 5 describes the visualization toolset.

2 World

The World System provides a physics based modeling and simulation for generating geometrically and radiometrically accurate mission data products. Geometric accuracy is defined as the accuracy of the apparent location, shape, and size of the observed bodies; Radiometric accuracy represents the accuracy of the contrast and absolute intensity level of the pixels in the simulated data products.

The world describes the properties of the bodies either targeted for observation or encountered during a mission. Properties include orbital dynamics, surface characteristics, and atmospheric dynamics. The list of target bodies and their relevant properties are described in a world configuration file. In the configuration file, a target body can be specified as one of the four body types: planet, satellite, asteroid, or comet. The configuration file is a high-level description of the world and it is connected to a phenomena model database which represents the phenomena in detail.

The main intent of the Phenomena Mode] Database is to establish a link to stat,c-of-the-art scientific knowledge so that the body of knowledge obtained from previous missions can be optimally utilized for future missions. The body of scientific knowledge includes measurements, models, hypotheses, etc. The major challenges in establishing the link are composition of a common representation frame, inconsistency verification, and accuracy/uncertainty measure specification, among others.

In the current Phenomena Model Database, a body is described employing three types of models: dynamics, geometric, and radiometric. A target body is desrcibed utilizing the geometric and radiometric models for solid body and/or gaseous body. For a body that has both attributes, such as a comet, the body can be described using both attributes. Detailed description of the models are presented below.

2.1 Dynamics Model

The dynamics model utilizes the PCK(Planet Constant Kernel) and SPK(Spacecraft and Planet Kernel) of the SPICE [2] format invented at JPL for archiving spacecraft states and mission events. The Object-Oriented SPICE library (OOSPICE) [3] is employed to propagate a body state for a specified time and reference coordinate system.

- *body rotation* — The Euler angles describe the orientation of the coordinate axes of the 'Body Equator and Prime Meridian' system with respect to the J2000 system. The three Euler angles are: the right ascension and declination of the north pole of a body as a function of time; and the prime meridian location which is expressed as a rotation about the north pole, also a function of time.
- *orbit dynamics* — The orbit dynamics file is generated by propagating the orbital elements – semi-major axis, eccentricity, inclination, longitude of the ascending node, argument of periapsis, true anomaly at a specified time, and gravitational force – using two-body Keplerian dynamics.

2.2 Geometric Model

The geometric model describes the shape of a target body at three levels of resolutions: general shape, surface topography, and roughness.

- *body shape* — The body shape is represented as a triaxial ellipsoid.

- *elevation map* — The elevation map represents the target body shape deviation from the triaxial ellipsoid body shape. It is generated from the polygonal representation of the target body which includes craters, volcanoes, and various geological features. It is used to compute the local slopes for more accurate photometric effects.

- *texture map* — The higher resolution surface topography is represented employing a surface texture map and it is used as an additional attenuation parameter in light intensity computation,

2.3 Radiometric Model

The radiometric model describes the reflectance characteristics of a target body for both solid surface and its atmospheric layer. Reflectance characteristics are modeled in both spatial and spectral dimensions.

- *albedo map* — The albedo map represents the reflectance distribution of the target body surface precomputed for a specified wavelength range.

- *material* map — The material map of a target body surface is represented with a material index map and a corresponding material name list. Material names are keys to the material spectral signature library composed for the World System.

- *atmospheric* dynamics — The photometric characteristics of a gaseous body or the gaseous part of a body (i.e., an atmosphere or a cometary coma), are described with a body specific material composition and a dynamics model provided by the science community.

3 Spacecraft System

For each encounter, an observation sequence is composed with the corresponding encounter profile which includes target body name, encounter duration, encounter geometry (closest approach time, distance, and velocity), a command sequence for data acquisition, and a command sequence for spacecraft's geometric state necessary for the data acquisition. During the observation sequence simulation, the Spacecraft System is responsible for interpreting and performing the commanded spacecraft's geometric states.

The geometric state includes spacecraft's position and velocity, and attitude control parameters derived for the desired data acquisition. Each geometric state has three representations of the state, predicted, true, and estimated. The predicted state indicates a state generated based on *a priori"* knowledge. The true state indicates the real state or achieved state of the spacecraft system after a command has been executed. The estimated state is the state analyzed by the spacecraft system on the achieved state.

The geometric state of a spacecraft is commanded based on the predicted and estimated states. The errors in prediction and estimation process can cause the valuable observation opportunities to be missed. The Spacecraft System plays a very important role in accurate analysis of their impacts and in developing an alternative observation scenario for ensuring the science return of the mission. For the DS1 encounter geometry simulation, a straight line trajectory and constant approach velocity were assumed for the spacecraft's position propagation. The following sections describe the attitude control modes and the three representations of the geometric state.

3.1 Attitude Control Modes

The attitude control is expressed employing four control modes in order to represent the desired pointing and slewing activities necessary for the data acquisition. The four ACS control modes are; cruise, track, pushbroom, and point.

In the cruise mode, ACS maintaining the current attitude.

In the track mode, ACS applies necessary attitude change to maintain the constant relative pointing to the specified target.

In the pushbroom mode, ACS applies the additional slew rate above the tracking to cover a desired target body area.

In the point mode, ACS supports for three types of pointing: target relative, absolute, and time-offset. The target relative pointing is specified with a target and off-nadir displacement. The absolute pointing is specified by a Quaternion. The time-based pointing is specified the time offset from the time of the closest approach. This is a special case of the absolute pointing where the Quaternion is internally computed for the specified time based on the trajectory information.

3.2 Predicted/Desired State

The geometric state of the spacecraft at a given time is expressed with three vectors: position(P), velocity(V), and attitude(@). For the asteroid encounter simulation, the time is expressed as a relative offset from the time of closest approach(T_{CA}) and the velocity is assumed to be constant. Thus the encounter geometry can be expressed as

$$t = T - T_{CA} \quad (1)$$

$$P(t) = P(T_{CA}) - Vt \quad (2)$$

where T is the J2000 inertial coordinate time.

$$\Phi = \begin{vmatrix} Ra \\ Dec \\ Twist \end{vmatrix} = \begin{bmatrix} \tan^{-1}(U_y^3/U_x^3) \\ \sin^{-1}(U_z^3) \\ \tan^{-1}(U_z^1/U_z^2) \end{bmatrix} \quad (3)$$

where

$$\begin{bmatrix} w \\ U^2 \\ U^3 \end{bmatrix} = \begin{bmatrix} (P\%V)\%P \\ P\%V \\ P \end{bmatrix} \quad (4)$$

where % indicates the cross product operation.

The angular acceleration is computed as the attitude change during one second interval as

$$\ddot{\Phi}(t) = \Phi(t+1) - \Phi(t) \quad (5)$$

When an additional angular distance or slew rate needs to be applied beyond the nadir pointing and tracking in order to support off-nadir detector pointing or pushbrooming observation, the additional angular acceleration and its duration must be kept track separately from the target tracking.

The additional acceleration and its duration is computed based on the commanded slew distance and the allowed acceleration beyond the tracking. The relationship between the additional slew distance (0), allowed time to travel the distance (t.), and applied angular acceleration ($\ddot{\theta}$) and its duration (t_a) can be expressed as

$$\theta = \ddot{\theta} t_a^2 + \dot{\theta}(t_e - 2t_a) \quad (6)$$

$$\dot{\theta} = \ddot{\theta} t_a \quad (7)$$

$$\ddot{\theta} < acc_{max} \quad (8)$$

Since the velocity is assumed to be constant during the encounter period, the predicted position at t refers to the position of the spacecraft at t' seconds before the predicted time of the closest approach.

$$t' = T - T_{CA}^P \quad (9)$$

$$P^P(t') = P^P(T_{CA}) - Vt' \quad (10)$$

where the superscript ^{P} indicates the predicted state and $P^P(T_{CA})$ indicates the predicted position at T_{CA}.

The desired attitude and angular acceleration profile for the required pointing at t seconds before the closest approach can be computed as

$$\Phi^D(t') = \Phi^P(t') + \theta \quad (11)$$

$$\ddot{\Phi}^D(t') = \ddot{\Phi}^P(t') + \ddot{\theta} \quad (12)$$

where the superscript ^{D} indicates the desired state and the predicted attitude($\Phi^P(t')$) indicates the attitude computed employing the predicted position and

It is important to note that the time t' is computed based on the predicted T_{CA}, which may not be the true T_{CA}. Thus the desired state acquired from the above process may be an erroneous state. The tolerable T_{CA} error(ϵ_t) range is discussed in section 4.2.

3.3 True/Achieved State

The true geometric state is the state the spacecraft is or achieved. The position is propagated based on time while the attitude is controlled based on the desired attitude. Thus, the true position is computed for the true time offset t while the true attitude is computed as the achieved attitude at the estimated time offset t' based on the desired attitude for that time as shown below.

$$P^T(t) = P(T_{CA}) - Vt \quad (13)$$

$$\Phi^T(t') = \Phi^D(t') + \epsilon_\Phi \quad (14)$$

where the superscript T indicates the true or achieved state.

The attitude error(ϵ_Φ) is the the angular distance traveled by the angular acceleration difference between the desired and applied during the 1 second control period. The difference is from the thrust power control resolution as expressed below.

$$\epsilon_\Phi = \ddot{\Phi}^D(t') - N(t')I \quad (15)$$

$$N(t') = \lceil \ddot{\Phi}^D(t')/E(I) \rceil \quad (16)$$

$$I = E(I) + G()\sigma_I \quad (17)$$

where $E(I)$ is the mean impulse size and $G()$ is the Gaussian random number generator with the value range between -5 and 5, σ_I is the one-sigma error of the impulse size.

The attitude error is referred to as *drift distance* and it is regulated by the ACS so that the error is within the specified limit. The regulation process and the range of the limit are referred to as *limit-cycling* and *deadband* respectively. Since the regulation is applied based on the estimated attitude error, the limit-cycling is discussed in the next section.

3.4 Estimated State

The estimated geometric state is the state the spacecraft analyzes its current state to be. For the DS1 asteroid encounter simulation, the estimated current state was analyzed to predict the time of the closest approach and the position at that time. Thus the estimation error was decoupled into T_{CA} error(ϵ_t) and target ephemeris error(ϵ_p) as

$$T_{CA}^P = T_C A + \epsilon_t \quad (18)$$

$$P^P(T_C A) = P_P(T_C A) + \epsilon_p \quad (19)$$

The errors were assumed to follow the Gaussian distribution and they were simulated using their one-σ error estimates as

$$\epsilon_p = G()\sigma_p$$

$$\epsilon_t = G()\sigma_t. \quad (21)$$

During the closest approach, when the angular acceleration changes rapidly, the T_{CA} error introduces very serious problem in target pointing and tracking due to the large angular acceleration error between the required and the predicted.

The estimated attitude is computed by applying the knowledge error to the achieved attitude.

$$\Phi^E(t') = \Phi^D(t') + \epsilon_\Phi + \epsilon_{acs} \quad (22)$$

The difference between the desired and the estimated attitude is referred to as estimated drift distance. When the estimated drift distance(p) is larger than the allowed drift limit (ρ_l) the attitude controller applies a minimum impulse in the opposite direction of the drift direction, which is referred to as *limit-cycling*. Assuming the process is repeated with one-second interval and the impulse can be applied instantaneously the process can be expressed as

$$\rho_i = \rho_{i-1} + \dot{\rho}_i + \epsilon_{acs} \quad (23)$$

$$\dot{\rho}_{i+1} = \dot{\rho}_i - I \quad \text{if } \rho_i > \rho_l \quad (24)$$

$$= \dot{\rho}_i + I \quad \text{if } \rho_i < -\rho_l \quad (25)$$

4 Camera Subsystem

During the observation sequence simulation, the Camera System is responsible for executing the data acquisition commands and synthesizing the corresponding mission data products. It is important to note that the spacecraft time is shared between the three components of the mission simulation. Thus, the operation timeline is interpreted based on the estimated T_{CA} not the true T_{CA} while the data products are synthesized for the true geometric state. The deviation between the estimated state and true state affects the apparent target position and size in the data products.

This section describes MICAS specific operation modes, the relationship between the geometric state accuracy and the instrument spec, and the role of ([20]) high fidelity scene generation in observation sequence design.

4.1 Operation Mode

The MICAS camera system is simulated for the following three types of operational modes. For each operation, the event start time is defined as the offset from the reference time. The timeline between exposure command and the attitude control command needs to be carefully coordinated in order to ensure the correct attitude has been achieved for the operation.

- snap — take one or more image frames with the specified detector and transfer the frames to the MICAS buffer. Detector ID, number of exposures, exposure duration, and time between exposures must be specified in this mode.
- *read-last* — transfer the image frame taken last from the MICAS buffer to the main memory system and save it in the spacecraft file system.
- *read-all* — transfer all of the image frames remaining in the MICAS buffer and save them in the spacecraft file system.

4.2 Spacecraft Performance Requirement

For each snap operation, the desired geometric state and tolerable error range for observing the target body are analyzed based on the scientific objectives. The scientific objectives vary for each target body and for each detector. For each objective, an optimal observation window may be defined to meet the required geometric relationship between the target body and the spacecraft.

The tolerable pointing inaccuracy during the encounter period can be expressed for two cases, before and after the apparent target size(S^a) exceeds the camera's field of view(F_v).

$$\Delta\Phi(t) = (F_v - rS^a(t))/2 \text{ if } S^a(t) <= F_v \quad (26)$$
$$= (S^a(t) - rF_v)/2 \text{ otherwise} \quad (27)$$

where r is the fraction of the target must be contained or the fraction of the camera's field of view that must be filled. The apparent target size is computed based on the maximum radius of the target body (R) and the distance of the target form the spacecraft.

$$S_T^a(t) = 2\tan\frac{R}{\sqrt{\| P(t) \|}} \quad (28)$$

The above relationship implies that the accuracy of the pointing performance requirement is tightly coupled with the instrument's FOV, navigation performance in estimating the TCA, and knowledge about the target body.

The tolerable pointing inaccuracy can be directly applied for pointing control error or translated into allowed T_{CA} error or target position error utilizing the fact that the attitude is a function of position and velocity at a specified time.

The allowed pointing control error range is expressed as

$$\sqrt{(\rho_l^2 + \epsilon_{acs}^2)} < \Delta\Phi \quad (29)$$

The allowed T_{CA} error range is expressed in terms of the closest time of approach estimate error (ϵ_t) which satisfies

$$|\Phi(t + \epsilon_t) - \Phi(t)| < \Delta\Phi. \quad (30)$$

And the allowed target position error range is expressed in terms of the Z directional position error (ϵ_p) which satisfies

$$|\Phi(P(t) + \epsilon_p, V) - \Phi(P(t), V)| < \Delta\Phi. \quad (31)$$

During a snap operation, the desired pointing stability is expressed as the maximum number of pixels that can be smeared during the exposure duration without distorting the scientific integrity of the data. The stability is represented with the target relative slew rate computed as

$$\dot{\theta} = (N f_v)/T_{exp} \quad (32)$$

where N is the number of pixels allowed to be smeared, f_v is the field of view of a pixel, and T_{exp}

is the exposure duration.

When the observation is performed in a pushbroom mode, the desired target relative slew rate is expressed as a function of the camera's FOV and exposure duration. The tolerable slew rate variation is determined by the range between the minimum overlapping required between the image slices and the overlap amount allowed for the maximum number of slices for constructing the target surface mosaic.

$$\epsilon_{\dot{\theta}} < \Delta r F_v / T_{exp} \quad (33)$$

$$\mathbf{A}\mathbf{r} = (r_{max} - r_{min})/2 \quad (34)$$

4.3 Scene Generation

Besides the geometric state and its tolerable variation required for the science observation, the intensity range of the observed target body must be carefully considered. The intensity range of an extended body is a function of the distance from the Sun, target albedo range, spacecraft orientation, instrument's sensitivity, and allowed exposure duration steps. Due to the interdependencies between the target phenomena and other subsystem performances, the observation sequence design for desired intensity range requires very accurate models and simulations of target body phenomena and the instrument system response characteristics.

For example, as shown in previous section, the exposure duration also plays an important role in setting the slew rate tolerance level. Thus, it cannot be arbitrarily set to satisfy the intensity range requirement. Also, when an instrument needs to be applied to several target bodies, each with different albedo range, the instrument's sensitivity cannot be altered easily. To make matters worse, the albedo range of target bodies may not be known *a priori.*

The mission simulation system provides a very high fidelity scene generation capability. The fidelity required for faint star position identification includes sub-pixel accuracy as well as sub-second accuracy simulation for optical blurring and spacecraft motion propagation. The scene generation [4] simulates the response/distortion characteristics of an instrument employing a camera system model. The model employs the following set of parameters:

. Optics — Point-Spread Function, Aperture size, F-number, Focal Length

- Detectors — Orientation, Offset, Type, Array size, Pixel size, Full well, Quantum efficiency, Dark current, CCD blooming and ghosting

- Electronics — A/D converter, Read noise

. Operation — exposure duration setting, read modes

The detector type includes monochrome and spectrometer. For both types of detectors, quantum efficiency can be specified as a function of wavelength. Figure 2 is an example data product constructed by a simulated CCD sensor of MICAS employing the asteroid phenomena database during a virtual asteroid encounter.

5 Mission Visualization

The mission simulation system is interfaced with a set of mission visualization tools for interactive control of the simulation process and monitoring of the progress. The tools were designed to monitor the simulation in a comprehensive manner by tracking the inter-component relations of the mission simulation system. The tools include three OpenInventor [5] based viewers: trajectory, spacecraft, and virtual camera. Each viewer is a stand-alone visualization tool generic to all space missions. The time coordination and state propagation is managed by the mission event handler.

The trajectory viewer monitors the relationship between the World and the Spacecraft System. The World includes stars, a subset of the solar system, target bodies, and spacecraft. The reference coordinate system, temporal resolution, and the viewing geometry can be dynamically set for an optimal viewing of the trajectory over the entire mission period. The trajectory visualizer employs OpenInventor Examiner for interactive 3D coordinate manipulation of the trajectory view. A snapshot of the trajectory visualization for the DS1 Spacecraft is illustrated in Figure 3.

The spacecraft viewer monitors the structural variation of the spacecraft including system orientation and articulated parts. It accepts the spacecraft structure model in OpenInventor format, and time stamped

3D position and orientation representation for the articulated parts. This viewer is also useful for monitoring the attitude changes that are too small for the trajectory viewer and too large for the virtual camera viewer.

The virtual camera viewer simulates a virtual wide-angle camera located at the spacecraft center for a view from the spacecraft. The wide-angle FOV may be designed to include the payload system's FOV when the geometric state of the spacecraft relative to the observed target body motion needs to be monitored. The wide-angle camera view is particularly useful when an instrument has multiple FOVs, as in the case of MICAS. Figure 4 illustrates the wide-angle view which includes the four sensors of MICAS. This view provides effective visualization of minute changes in spacecraft state during the payload sequence execution that are not visible from the spacecraft viewer.

6 Summary

The mission simulation system software was proven to be a very effective platform for integrating various aspects of mission design, analyzing their impacts to the science return, and discussing the design trade-off options. The DS1/MICAS asteroid encounter observation sequence simulation made a significant contribution in making major mission operation decisions.

The main emphases of the current implementation are to realistically synthesize the integrated performance of MICAS, ACS, and OpNav, and to analyze the impacts of the uncertainties/errors in target models, MICAS response characteristics, ACS performance, and OpNAV accuracy. The system is being extended to assist in design and validation of the observation sequences for West-Kohoutek-Ikemura comet encounter, Mars encounter, and periodic MICAS calibrations for in-depth technology validation.

7 Acknowledgement

This work was performed at the Jet Propulsion Laboratory, California Institute of Technology, under contract with the National Aeronautics and Space Administration. The funding was provided by the information systems branch of Code STI/NASA, JPL flight system testbed, and MICAS/New Millennium project.

References

[1] Amit Sen, *Interface Control Document & Product Functional Specification Document,* Sept, '96, NMP DS1 6446-464, JPL internal documentation D-13543

[2] Charles Acton, Jr., *Ancillary Data Services of NASA's Navigation and* Ancillary *Information Facility,* Planetary and Space Sciences, Vol. 44, No. 1 PP 65-70, 1996

[3] Richard Weidner, *Object-Oriented SPICE Library,* http: //spartacus/richard

[4] Meemong Lee, Raymond Swartz, Richard Weidner, SceneGen, JPL New Technology Report No. 20053/0685

[5] OpenInventor Architecture Group, *OpenInventor C++ Reference* Manual, Release 2, Addison-Wesley Publishing Company.

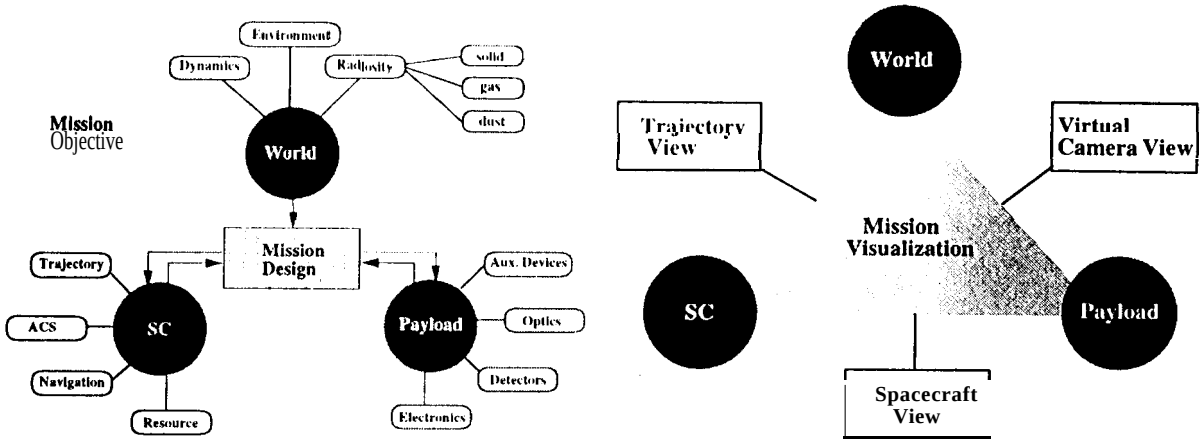

Figure 1. Mission Simulation and Visualization

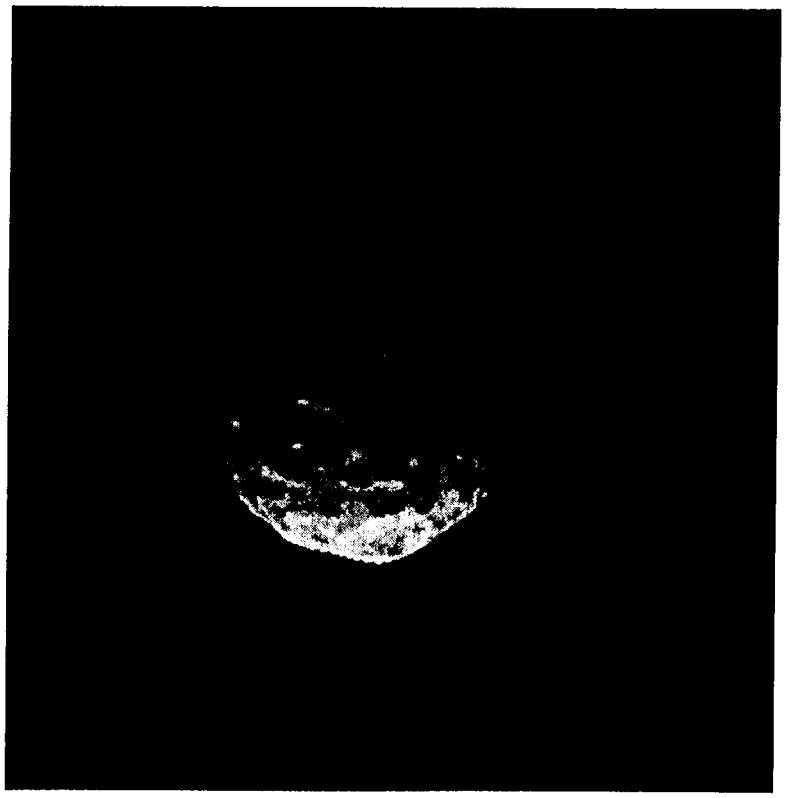

Figure 2. Target Asteroid Image Acquired by the CCD Sensor of MICAS

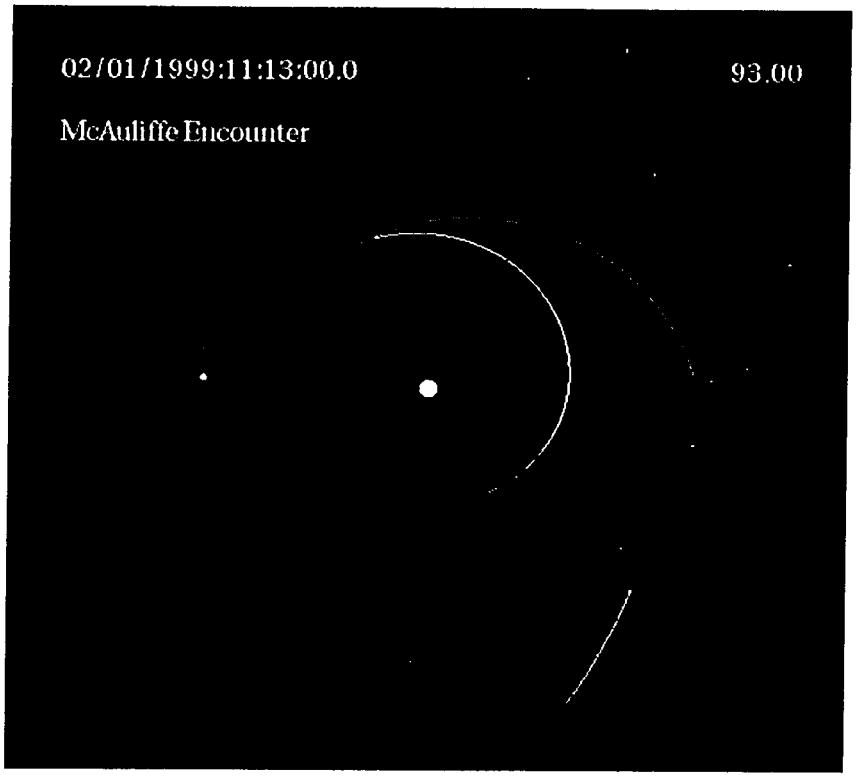

Figure 3. Snapshot of DS1 Spacecraft Trajectory Visualization

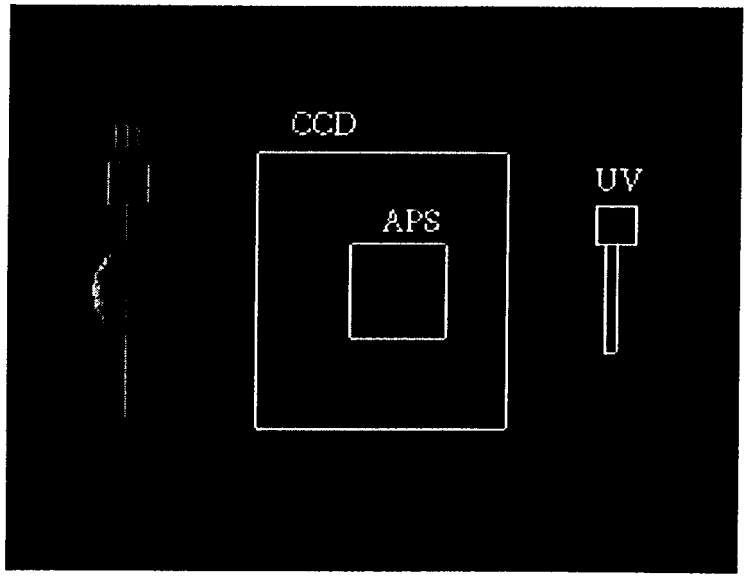

Figure 4. Geometric Alignment of Fields-of-View of Four Sensors **of MICAS**

ENCOUNTER GEOMETRY AND SCIENCE DATA GATHERING SIMULATION

Meemong Lee
Raymond L. Swartz
Ansel Teng
Richard J. Weidner

Jet Propulsion Laboratory
California Institute of Technology
4800 Oak Grove Dr., Pasadena Ca. 91109

Abstract

Each space mission follows the process cycle of design, development, integration and test, launch and operation, science analysis and archive. The desire for more frequent and cost effective missions has motivated various new research and development efforts to reduce the design to launch period and the operation/analysis costs. With the revolutionary advances in information technology, the role of software simulation is becoming a very significant part of that pursuit. This paper presents a mission simulation software applied for design and validation of the MICAS observation sequence during the Deep Space 1 mission(DS1) of the New Millennium project . The mission simulation software integrates three systems, world, spacecraft, and observation system, in a distributed computing environment. The three systems are coordinated with a set of mission visualization tools for interactive control and comprehensive monitoring of the simulated mission. Major advantages of the integrated simulation system include inter-subsystem dependency and integrated impact simulation, subsystem-level performance requirement analysis, controlled propagation of subsystem-level uncertainties/errors, and high-fidelity mission data product generation.

1 Introduction

Modeling and Simulation is a fundamental part of scientific methods, which has guided the evolution of the science discipline. Modeling provides the continuity in science endeavor as a mechanism to express beliefs, hypotheses, or imaginations, to organize the current understandings, to analyze the observed phenomena, to predict future outcomes, and to update new discoveries.

Though the importance of modeling and simulation in mission design has been well acknowledged, a comprehensive system-level modeling and simulation was not feasible until recently. With the recent revolutionary advances in information technology in terms of computational power, computer graphics, and networking, modeling and simulation are becoming cost-effective tools for larger and more complex system design.

Mission Simulation and Instrument Modeling group at JPL, has been developing a comprehensive mission simulation software system [1] for generic science observation sequence design and validation. The mission simulation has been applied to several missions including Stardust/Discovery, Second Generation Micro-Spacecraft, and DS1 /NewMillennium.

This paper discusses the mission simulation applied for DS1/MICAS observation sequence design and validation. The DS1 mision is planned to encounter an asteroid (McAulliffe), Mars, and a comet (West-Kohoutek-Ikemura) during the two year mission period. The MICAS (Miniature Imaging Camera and Spectrometer) [1] is a primary payload system of the DS1 mission. MICAS has four detectors sharing the same optics: CCD (Charge-Coui~lcd

Device), APS (Active Pixel Sensor), UV (Ultraviolet, Spectrometer), and IR (Infrared Spectrometer). The effective field of views of the four detectors and their geometric relationship can be seen in the virtual camera view displayed in section 5.

Figure 1 depicts the relationship between the mission simulation and visualization. The mission simulation system is composed of three components: *World, Spacecraft,* and *Payload (Camera).* The three components contribute toward achieving the mission objective: *World,* the phenomena of the physical world the payload system will observe; *Spacecraft,* the geometric state control and estimation; and *Payload (Camera),* the observing system's performance and data product synthesis, Mission visualization monitors the inter-component relationship during the simulation employing three interactivel y controlled visualizers: trajectory, spacecraft, and virtual camera. The Sections 2, 3,and 4 discusses the three components of the mission simulation system in relation to encounter geometry and science data gathering simulation and the section 5 describes the visualization toolset.

2 World

The World System provides a physics based modeling and simulation for generating geometrically and radiometrically accurate mission data products. Geometric accuracy is defined as the accuracy of the apparent location, shape, and size of the observed bodies; Radiometric accuracy represents the accuracy of the contrast and absolute intensity level of the pixels in the simulated data products.

The world describes the properties of the bodies either targeted for observation or encountered during a mission. Properties include orbital dynamics, surface characteristics, and atmospheric dynamics. The list of target bodies and their relevant properties are described in a world configuration file. In the configuration file, a target body can be specified as one of the four body types: planet, satellite, asteroid, or comet. The configuration file is a high-level description of the world and it is connected to a phenomena model database which represents the phenomena in detail.

The main intent of the Phenomena Model Database is to establish a link to state-of-the-art scientific knowledge so that the body of knowledge obtained from previous missions can be optimally utilized for future missions. The body of scientific knowledge includes measurements, models, hypotheses, etc. The major challenges in establishing the link are composition of a common representation frame, inconsistency verification, and accuracy/uncertainty measure specification, among others.

In the current Phenomena Model Database, a body is described employing three types of models: dynamics, geometric, and radiometric. A target body is desrcibed utilizing the geometric and radiometric models for solid body and/or gaseous body. For a body that has both attributes, such as a comet, the body can be described using both attributes. Detailed description of the models are presented below.

2.1 Dynamics Model

The dynamics model utilizes the PCK(Planet Constant Kernel) and SPK(Spacecraft and Planet Kernel) of the SPICE [2] format invented at JPL for archiving spacecraft states and mission events. The Object-Oriented SPICE library (OOSPICE) [3] is employed to propagate a body state for a specified time and reference coordinate system.

- *body rotation* — The Euler angles describe the orientation of the coordinate axes of the 'Body Equator and Prime Meridian' system with respect to the J2000 system. The three Euler angles are: the right ascension and declination of the north pole of a body as a function of time; and the prime meridian location which is expressed as a rotation about the north pole, also a function of time.

- *orbit dynamics* — The orbit dynamics file is generated by propagating the orbital elements – semi-major axis, eccentricity, inclination, longitude of the ascending node, argument of periapsis, true anomaly at a specified time, and gravitational force – using two-body Keplerian dynamics.

2.2 Geometric Model

The **geometric model describes** the shape of a target body at three levels of resolutions: general shape, surface topography, and roughness.

- *body shape* — The body shape is represented as a triaxial ellipsoid.

- *elevation map* — The elevation map represents the target body shape deviation from the triaxial ellipsoid body shape. It is generated from the polygonal representation of the target body which includes craters, volcanoes, and various geological features. It is used to compute the local slopes for more accurate photometric effects.

- *texture map* — The higher resolution surface topography is represented employing a surface texture map and it is used as an additional attenuation parameter in light intensity computation.

2.3 Radiometric Model

The radiometric model describes the reflectance characteristics of a target body for both solid surface and its atmospheric layer. Reflectance characteristics are modeled in both spatial and spectral dimensions.

- *albedo map* — The albedo map represents the reflectance distribution of the target body surface precomputed for a specified wavelength range.

- *material map* — The material map of a target body surface is represented with a material index map and a corresponding material name list. Material names are keys to the material spectral signature library composed for the World System.

- *atmospheric dynamics* — The photometric characteristics of a gaseous body or the gaseous part of a body (i.e., an atmosphere or a cometary coma), are described with a body specific material composition and a dynamics model provided by the science community.

3 Spacecraft System

For each encounter, an observation sequence is composed with the corresponding encounter profile which includes target body name, encounter duration, encounter geometry (closest approach time, distance, and velocity), a command sequence for data acquisition, and a command sequence for spacecraft's geometric state necessary for the data acquisition. During the observation sequence simulation, the Spacecraft System is responsible for interpreting and performing the commanded spacecraft's geometric states.

The geometric state includes spacecraft's position and velocity, and attitude control parameters derived for the desired data acquisition. Each geometric state has three representations of the state, predicted, true, and estimated. The predicted state indicates a state generated based on a *priori* knowledge. The true state indicates the real state or achieved state of the spacecraft system after a command has been executed. The estimated state is the state analyzed by the spacecraft system on the achieved state.

The geometric state of a spacecraft is commanded based on the predicted and estimated states. The errors in prediction and estimation process can cause the valuable observation opportunities to be missed. The Spacecraft System plays a very important role in accurate analysis of their impacts and in developing an alternative observation scenario for ensuring the science return of the mission. For the DS1 encounter geometry simulation, a straight line trajectory and constant approach velocity were assumed for the spacecraft's position propagation. The following sections describe the attitude control modes and the three representations of the geometric state.

3.1 Attitude Control Modes

The attitude control is expressed employing four control modes in order to represent the desired pointing and slewing activities necessary for the data acquisition. The four ACS control modes are; cruise, track, pushbroom, and point.

In the cruise mode, ACS maintaining the current attitude.

In the track mode, ACS applies necessary attitude change to maintain the constant relative pointing to the specified target.

In the pushbroom mode, ACS applies the additional slew rate above the tracking to cover a desired target body area.

In the point mode, ACS supports for three types of pointing: target relative, absolute, and time-offset. The target relative pointing is specified with a target and off-nadir displacement. The absolute pointing is specified by a Quaternion. The time-based pointing is specified the time offset from the time of the closest approach. This is a special case of the absolute pointing where the Quaternion is internally computed for the specified time based 011 the trajectory information.

3.2 Predicted/Desired State

The geometric state of the spacecraft at a given time is expressed with three vectors: position(P), velocity(V), and attitude(Φ). For the asteroid encounter simulation, the time is expressed as a relative offset from the time of closest approach (T_{CA}) and the velocity is assumed to be constant. Thus the encounter geometry can be expressed as

$$t = T - T_{CA} \quad (1)$$

$$P(t) = P(T_{CA}) - Vt \quad (2)$$

where T is the J2000 inertial coordinate time.

$$\Phi = \begin{vmatrix} \text{Ra} \\ \text{L3ec} \\ \textit{Twist} \end{vmatrix} = \begin{bmatrix} \tan^{-1}(U_y^3/U_x^3) \\ \sin^{-1}(U_z^3) \\ \tan^{-1}(U_z^1/U_z^2) \end{bmatrix} \quad (3)$$

where

$$\begin{bmatrix} U^1 \\ U^2 \\ U^3 \end{bmatrix} = \begin{bmatrix} (P\%V)\%P \\ P\%V \\ P \end{bmatrix} \quad (4)$$

where % indicates the cross product operation.

The angular acceleration is computed as the attitude change during one second interval as

$$\ddot{\Phi}(t) = \Phi(t+1) - \Phi(t) \quad (5)$$

When an additional angular distance or slew rate needs to be applied beyond the nadir pointing and tracking in order to support off-nadir detector pointing or pushbrooming observation, the additional angular acceleration and its duration must be kept track separately from the target tracking.

The additional acceleration and its duration is computed based on the commanded slew distance and the allowed acceleration beyond the tracking. The relationship between the additional slew distance (0), allowed time to travel the distance (t_e), and applied angular acceleration (θ) and its duration (t_a) can be expressed as

$$\theta = \ddot{\theta} t_a^2 + \dot{\theta}(t_e - 2t_a) \quad (6)$$

$$\dot{\theta} = \ddot{\theta} t_a \quad (7)$$

$$\ddot{\theta} < acc_{max} \quad (8)$$

Since the velocity is assumed to be constant during the encounter period, the predicted position at t refers to the position of the spacecraft at t' seconds before the predicted time of the closest approach.

$$t' = T - T_{CA}^P \quad (9)$$

$$P^P(t') = P^P(T_{CA}) - Vt' \quad (10)$$

where the superscript ^{P} indicates the predicted state and $P^P(T_{CA})$ indicates the predicted position at T_{CA}.

The desired attitude and angular acceleration profile for the required pointing at t seconds before the closest approach can be computed as

$$\Phi^D(t') = \Phi^P(t') + \theta \quad (11)$$

$$\ddot{\Phi}^D(t') = \ddot{\Phi}^P(t') + \ddot{\theta} \quad (12)$$

where the superscript ^{D} indicates the desired state and the predicted attitude($\Phi^P(t')$) indicates the attitude computed employing the predicted position and

It is important to note that the time t' is computed based on the predicted T_{CA}, which may not be the true T_{CA}. Thus the desired state acquired from the above process may be an erroneous state. The tolerable T_{CA} error(ϵ_t) range is discussed in section 4.2.

3.3 True/Achieved State

The true geometric state is the state the spacecraft is or achieved. The position is propagated based on time while the attitude is controlled based on the desired attitude. Thus, the true position is computed for the true time offset t while the true attitude is computed as the achieved attitude at the estimated time offset t' based on the desired attitude for that time as shown below.

$$P^T(t) = P(T_{CA}) - Vt \quad (13)$$

$$\Phi^T(t') = \Phi^D(t') + \epsilon_\Phi \quad (14)$$

where the superscript ^{T} indicates the true or achieved state.

The attitude error(ϵ_Φ) is the the angular distance traveled by the angular acceleration difference between the desired and applied during the 1 second control period. The difference is from the thrust power control resolution as expressed below.

$$\epsilon_\Phi = \ddot{\Phi}^D(t') - N(t')I \quad (15)$$

$$N(t') = \lceil \ddot{\Phi}^D(t')/E(I) \rceil \quad (16)$$

$$I = E(I) + G()\sigma_I \quad (17)$$

where $E(I)$ is the mean impulse size and $G()$ is the Gaussian random number generator with the value range between -5 and 5, σ_I is the one-sigma error of the impulse size.

The attitude error is referred to as *drift distance* and it is regulated by the ACS so that the error is within the specified limit. The regulation process and the range of the limit are referred to as *limit-cycling* and *deadband* respectively. Since the regulation is applied based on the estimated attitude error, the *limit-cycling* is discussed in the next section.

3,4 Estimated State

The estimated geometric state is the state the spacecraft analyzes its current state to be. For the DS1 asteroid encounter simulation, the estimated current state was analyzed to predict the time of the closest approach and the position at that time. Thus the estimation error was decoupled into T_{CA} error(ϵ_t) and target ephemeris error(ϵ_p) as

$$T_{CA}^P = T_C A + \epsilon_t \quad (18)$$

$$P^P(T_C A) = P_P(T_C A) + \epsilon_p \quad (19)$$

The errors were assumed to follow the Gaussian distribution and they were simulated using their one-σ error estimates as

$$\epsilon_p = G()\sigma_p \quad (20)$$

$$\epsilon_t = G()\sigma_t. \quad (21)$$

During the closest approach, when the angular acceleration changes rapidly, the T_{CA} error introduces very serious problem in target pointing and tracking due to the large angular acceleration error between the required and the predicted.

The estimated attitude is computed by applying the knowledge error to the achieved attitude.

$$\Phi^E(t') = \Phi^D(t') + \epsilon_\Phi + \epsilon_{acs} \quad (22)$$

The difference between the desired and the estimated attitude is referred to as estimated drift distance. When the estimated drift distance(p) is larger than the allowed drift limit (ρ_l) the attitude controller applies a minimum impulse in the opposite direction of the drift direction, which is referred to as limit-cycling. Assuming the process is repeated with one-second interval and the impulse can be applied instantaneously the process can be expressed as

$$Pi = \rho_{i-1} + \dot{\rho}_i + \epsilon_{acs} \quad (23)$$

$$\dot{\rho}_{i+1} = \dot{\rho}_i - I \quad \text{if } \rho_i > \rho_l \quad (24)$$

$$= \dot{\rho}_i + I \quad \text{if } \rho_i < -\rho_l \quad (25)$$

4 Camera Subsvstem

During the observation sequence simulation, the Camera System is responsible for executing the data acquisition commands and synthesizing the corresponding mission data products. It is important to note that the spacecraft time is shared between the three components of the mission simulation. Thus, the operation timeline is interpreted based on the estimated T_{CA} not the true T_{CA} while the data products are synthesized for the true geometric state. The deviation between the estimated state and true state affects the apparent target position and size in the data products.

This section describes MICAS specific operation modes, the relationship between the geometric state accuracy and the instrument spec, and the role of high fidelity scene generation in observation sequence design.

4.1 Operation Mode

The MICAS camera system is simulated for the following three types of operational modes. For each operation, the event start time is defined as the offset from the reference time. The timeline between exposure command and the attitude control command needs to be carefully coordinated in order to ensure the correct attitude has been achieved for the operation.

- snap — take one or more image frames with the specified detector and transfer the frames to the MICAS buffer. Detector ID, number of exposures, exposure duration, and time between exposures must be specified in this mode.
- *read-last* — transfer the image frame taken last from the MICAS buffer to the main memory system and save it in the spacecraft file system.
- read-all — transfer all of the image frames remaining in the MICAS buffer and save them in the spacecraft file system.

4.2 Spacecraft Performance Requirement

For each snap operation, the desired geometric state and tolerable error range for observing the target body are analyzed based on the scientific objectives. The scientific objectives vary for each target body and for each detector. For each objective, an optimal observation window may be defined to meet the required geometric relationship between the target body and the spacecraft.

The tolerable pointing inaccuracy during the encounter period can be expressed for two cases, before and after the apparent target size(S^a) exceeds the camera's field of view(F_v).

$$\Delta\Phi(t) = (F_v - rS^a(t))/2 \text{ if } S^a(t) <= F_v \quad (26)$$
$$= (S^a(t) - rF_v)/2 \text{ otherwise} \quad (27)$$

where r is the fraction of the target must be contained or the fraction of the camera's field of view that must be filled. The apparent target size is computed based on the maximum radius of the tar-got body (R) and the distance of the target form the spacecraft.

$$S_T^a(t) = 2\tan\frac{R}{\sqrt{\| P(t) \|}} \quad (28)$$

The above relationship implies that the accuracy of the pointing performance requirement is tightly coupled with the instrument's FOV, navigation performance in estimating the TCA, and knowledge about the target body.

The tolerable pointing inaccuracy can be directly applied for pointing control error or translated into allowed T_{CA} error or target position error utilizing the fact that the attitude is a function of position and velocity at a specified time.

The allowed pointing control error range is expressed as

$$\sqrt{(\rho_l^2 + \epsilon_{acs}^2)} < \Delta\Phi \quad (29)$$

The allowed T_{CA} error range is expressed in terms of the closest time of approach estimate error (ϵ_t) which satisfies

$$|\Phi(t + \epsilon_t) - \Phi(t)| < \Delta\Phi. \quad (30)$$

And the allowed target position error range is expressed in terms of the Z directional position error (ϵ_p) which satisfies

$$|\Phi(P(t) + \epsilon_p, V) - \Phi(P(t), V)| < \Delta\Phi. \quad (31)$$

During a snap operation, the desired pointing stability is expressed as the maximum number of pixels that can be smeared during the exposure duration without distorting the scientific integrity of the data. The stability is represented with the target relative slew rate computed as

$$\dot{\theta} = (Nf_v)/T_{exp} \quad (32)$$

where N is the number of pixels allowed to be smeared, f_v is the field of view of a pixel, and T_{exp}

is the exposure duration.

When the observation is performed in a pushbroom mode, the desired target relative slew rate is expressed as a function of the camera's FOV and exposure duration. The tolerable slew rate variation is determined by the range between the minimum overlapping required between the image slices and the overlap amount allowed for the maximum number of slices for constructing the target surface mosaic.

$$\epsilon_{\dot{\theta}} < \Delta r F_v / T_{exp} \quad (33)$$

$$\mathrm{Ar} = (r_{max} - r_{min})/2 \quad (34)$$

4.3 Scene Generation

Besides the geometric state and its tolerable variation required for the science observation, the intensity range of the observed target body must be carefully considered. The intensity range of an extended body is a function of the distance from the Sun, target albedo range, spacecraft orientation, instrument's sensitivity, and allowed exposure duration steps. Due to the interdependencies between the target phenomena and other subsystem performances, the observation sequence design for desired intensity range requires very accurate models and simulations of target body phenomena and the instrument system response characteristics.

For example, as shown in previous section, the exposure duration also plays an important role in setting the slew rate tolerance level. Thus, it cannot be arbitrarily set to satisfy the intensity range requirement. Also, when an instrument needs to be applied to several target bodies, each with different albedo range, the instrument's sensitivity cannot be altered easily. To make matters worse, the albedo range of target bodies may not be known *a priori.*

The mission simulation system provides a very high fidelity scene generation capability. The fidelity required for faint star position identification includes sub-pixel accuracy as well as sub-second accuracy simulation for optical blurring and spacecraft motion propagation. The scene generation [4] simulates the response/distortion characteristics of an instrument employing a camera system model. The model employs the following set of parameters:

- Optics — Point-Spread Function, Aperture size, F-number, Focal Length
- Detectors — Orientation, Offset, Type, Array size, Pixel size, Full well, Quantum efficiency, Dark current, CCD blooming and ghosting
- Electronics — A/D converter, Read noise
- Operation — exposure duration setting, read modes

The detector type includes monochrome and spectrometer. For both types of detectors, quantum efficiency can be specified as a function of wavelength. Figure 2 is an example data product constructed by a simulated CCD sensor of MICAS employing the asteroid phenomena database during a virtual asteroid encounter.

5 Mission Visualization

The mission simulation system is interfaced with a set of mission visualization tools for interactive control of the simulation process and monitoring of the progress. The tools were designed to monitor the simulation in a comprehensive manner by tracking the inter-component relations of the mission simulation system. The tools include three OpenInventor [5] based viewers: trajectory, spacecraft, and virtual camera. Each viewer is a stand-alone visualization tool generic to all space missions. The time coordination and state propagation is managed by the mission event handler.

The trajectory viewer monitors the relationship between the World and the Spacecraft System. The World includes stars, a subset of the solar system, target bodies, and spacecraft. The reference coordinate system, temporal resolution, and the viewing geometry can be dynamically set for an optimal viewing of the trajectory over the entire mission period. The trajectory visualizer employs OpenInventor Examiner for interactive 3D coordinate manipulation of the trajectory view. A snapshot of the trajectory visualization for the DS1 Spacecraft is illustrated in Figure 3.

The spacecraft viewer monitors the structural variation of the spacecraft including system orientation and articulated parts. It accepts the spacecraft structure model in OpenInventor format and time stamped

3D position and orientation representation for the articulated parts. This viewer is also useful for monitoring the attitude changes that are too small for the trajectory viewer and too large for the virtual camera viewer.

The virtual camera viewer simulates a virtual wide-angle camera located at the spacecraft center for a view from the spacecraft. The wide-angle FOV may be designed to include the payload system's FOV when the geometric state of the spacecraft relative to the observed target body motion needs to be monitored. The wide-angle camera view is particularly useful when an instrument has multiple FOVS, as in the case of MICAS. Figure 4 illustrates the wide-angle view which includes the four sensors of MICAS. This view provides effective visualization of minute changes in spacecraft state during the payload sequence execution that are not visible from the spacecraft viewer.

6 Summary

The mission simulation system software was proven to be a very effective platform for integrating various aspects of mission design, analyzing their impacts to the science return, and discussing the design trade-off options. The DS1/MICAS asteroid encounter observation sequence simulation made a significant contribution in making major mission operation decisions.

The main emphases of the current implementation are to realistically synthesize the integrated performance of MICAS, ACS, and OpNav, and to analyze the impacts of the uncertainties/errors in target models, MICAS response characteristics, ACS performance, and OpNAV accuracy. The system is being extended to assist in design and validation of the observation sequences for West-Kohoutek-Ikemura comet encounter, Mars encounter, and periodic MICAS calibrations for in-depth technology validation.

7 Acknowledgement

This work was performed at the Jet Propulsion Laboratory, California Institute of Technology, under contract with the National Aeronautics and Space Administration. The funding was provided by the information systems branch of Code STI/NASA, JPL flight system testbed, and MICAS/New Millennium project.

References

[1] Amit Sen, *Interface Control* Document *& Product Functional Specification Document,* Sept, '96, NMP DS1 6446-464, JPL internal documentation D-13543

[2] Charles Acton, Jr., *Ancillary Data Services of NASA's* Navigation *and Ancillary Information Facility,* Planetary and Space Sciences, Vol. 44, No. 1 PP 65-70, 1996

[3] Richard Weidner, *Object-Oriented SPICE* Li*brary,* http: //spartacus/ richard

[4] Meemong Lee, Raymond Swartz, Richard Weidner, SceneGen, JPL New Technology Report No. 20053/0685

[5] OpenInventor Architecture Group, *OpenInventor C++ Reference Manual,* Release 2, Addison-Wesley Publishing Company.

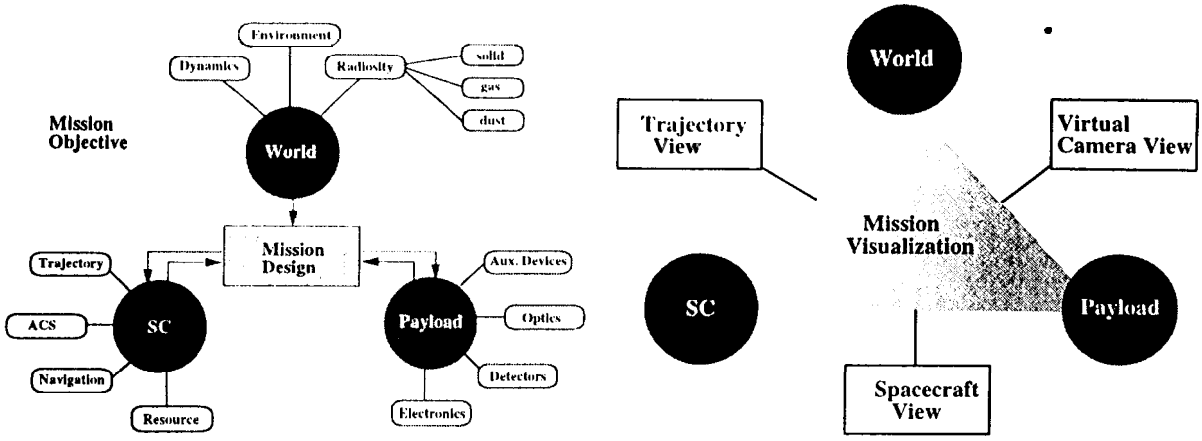

Figure 1. Mission Simulation and Visualization

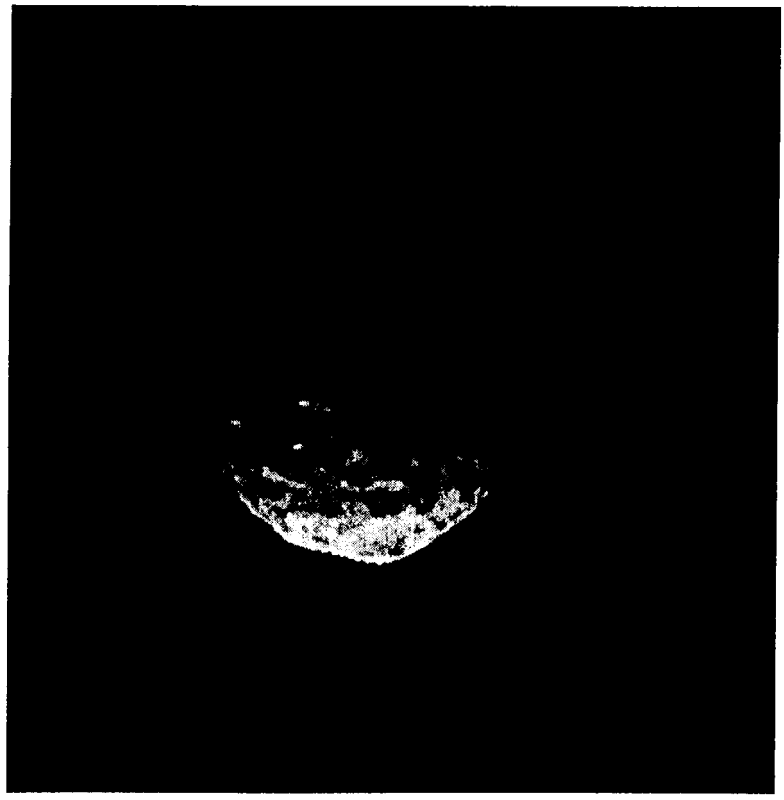

Figure 2. Target Asteroid Image Acquired by the CCD Sensor of MICAS

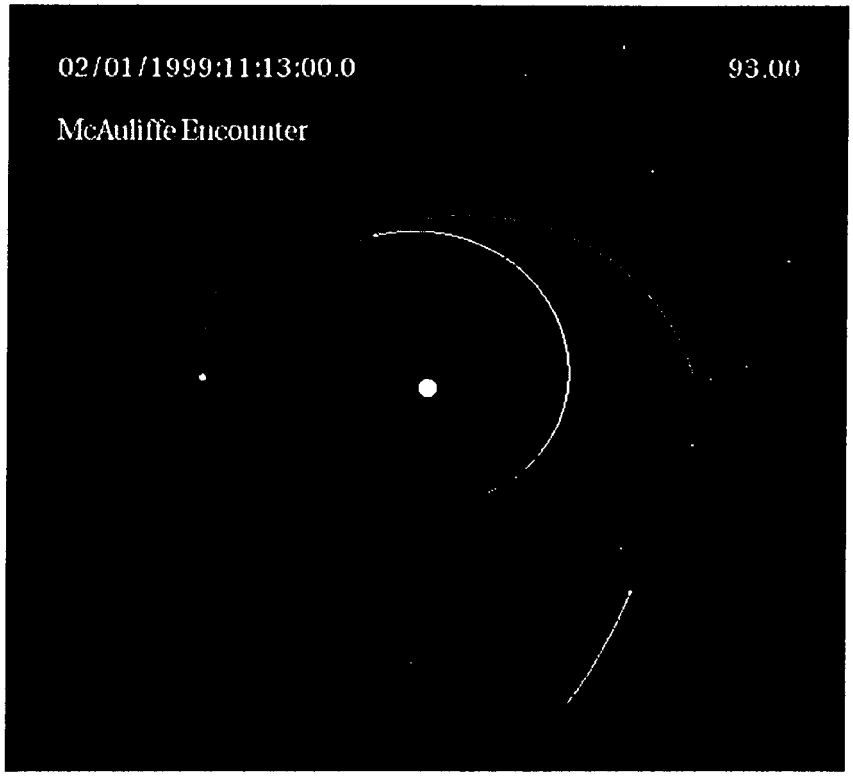

Figure 3. Snapshot of DS1 Spacecraft Trajectory Visualization

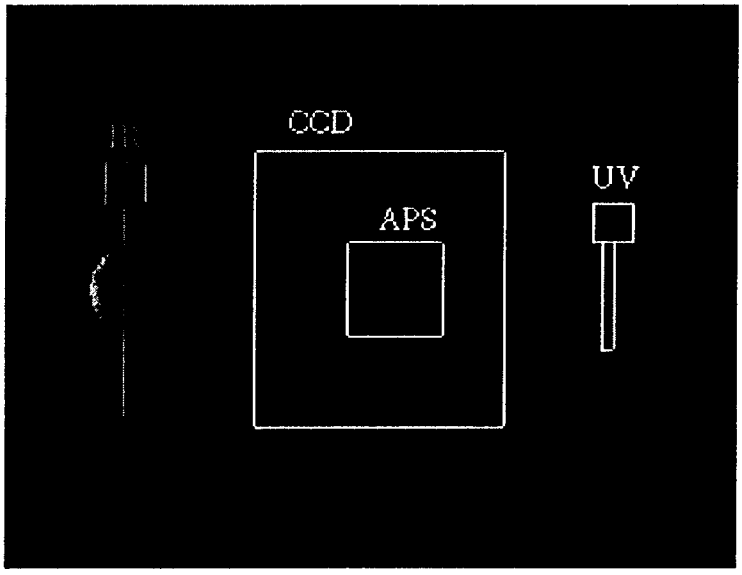

Figure 4. Geometric Alignment of Fields-of-View of Four Sensors of MICAS